

Synthesis of Carbon black/geopolymer composites with high and stable electrothermal performance

Sibtt Mohammed Jabbar, Dalya Hekmat Hameed, and Imad Ali Disher*

Department of Ceramics and Building Materials, College of Materials Engineering, University of Babylon, Babil, Iraq.

*Corresponding Author:

E-mail Address: imadali4@uobabylon.edu.iq

Abstract

Geopolymer/nano carbon black composite is a promising electrically conductive smart material that can be used in self-heating and self-sensing applications. This paper studies the effect of adding nano carbon black to the physical, mechanical, electrical, and electrothermal performance of metakaolin-based geopolymer. Carbon black was added at the percent of 5%, 10%, 15%, and 20% by weight of metakaolin; the compressive strength was tested at various ages of 7, 14, 28, and 90 days, and the electrothermal performance was tested using AC and DC voltages. The results showed that a compromise between suitable compressive strength and high electrothermal conversion could be achieved when a specific balance between the carbon black percent and the lowest water content is established. A composite with a compressive strength of 27 MPa and stable electrothermal performance reaching 142°C at 9V DC can be prepared using 20 wt% of carbon black and a water-to-metakaolin ratio of 0.549, which is used as a smart material in construction applications.

Keywords: Geopolymer, Nano carbon black, Metakaolin, Electrothermal, Self-heating, Smart materials.

24 1. Introduction

25 Geopolymer is a promising alternative to ordinary Portland cement, which is a traditional building
26 material [1]. It is characterized by its resistance to high temperature and corrosion [2,3], high
27 mechanical performance and high durability [4–6]. Also, it is an environmentally friendly material
28 due to the low emission of CO₂ gas from its production processes [7,8]. Because of its unique
29 properties, geopolymer can be used in construction applications as well as in many other
30 applications, such as heavy metal immobilization [9–11], coating applications [12], and fire
31 resistance applications [13].

32 Geopolymer is manufactured from raw materials rich in alumina and silica after mixing with an
33 alkaline solution. Geopolymer materials are generally formed by three types of polysialate 3D
34 networks consisting of SiO₄ and AlO₄ tetrahedrons, which are polysialate (-Si-O-Al-O-),
35 polysialate-siloxo (-Si-O-Al-O-Si-O-) and polysialate-disiloxo (-Si-O-Al-O-Si-O-Si-O-). The
36 cavities within these networks are filled by corresponding cations (Na⁺, K⁺, Ca⁺⁺, and Cs⁺)
37 contributing to balancing the negative charge for Al⁺³ [14]. The performance of geopolymer
38 depends mainly on the properties of its raw materials; metakaolin is considered one of the best
39 precursors for manufacturing geopolymer due to its high fraction of silica and alumina, low
40 impurities, stable chemical composition, and high purity compared to fly ash and slag [15–17].

41 Carbon black is a substance that is difficult to dispose of and is produced from various industrial
42 processes as byproducts, in the form of a fine powder containing a high percentage of carbon; it is
43 characterized by high specific surface area, high chemical and thermal stability, and good electrical
44 conductivity, also this waste is usually decomposed into landfills causing soil contamination and
45 water pollution [18].

46 Geopolymer is not electrically conductive in its dry state, so carbon black can be added to improve
47 its electrical conductivity, and thus, it becomes a material that can be used in self-heating [19] and

48 self-sensing [20] applications. Carbon black cannot be added in high proportions due to the
49 negative effect on the mechanical properties [19,21,22].

50 Many studies have dealt with adding carbon black to improve the electric performance of
51 geopolymers. Arif et al. made a composite material from geopolymer with the inclusion of carbon
52 black to be used as an X-ray shield [23]. Rauf et al. added carbon black with Fe₃O₄ to improve the
53 electrical and optical properties and gamma ray absorption of the geopolymer [24]. Gu et al. added
54 nanocarbon black with carbon fibers to improve the electrothermal performance of geopolymers
55 used in paving Airports [25]. Han et al. found that adding 15 vol% and 0.05 vol% of both nano
56 carbon black and carbon fibers to the geopolymer gives the best result in terms of electrical
57 conductivity [26]. Mizerová et al. studied the effect of adding carbon black, at a percentage not
58 exceeding 2% by weight of fly ash, on the self-sensing property of geopolymer [27]. Irshidat et
59 al. studied the effect of adding carbon black at percentages of 5%-40% by weight of fly ash on the
60 mechanical and physical properties of geopolymer; they found that adding carbon black at 5% and
61 20% leads to an increase in compressive strength to 46.89 and 45.9 MPa, respectively, compared
62 to the compressive strength of the reference sample at 44.79 MPa [18]. Cai et al. studied the effect
63 of self-heating on accelerating the curing of geopolymer by adding carbon black and steel fibers
64 at 6 and 2 vol%, respectively; they obtained a sample with the unstable electrothermal performance
65 of 67°C at 110 DC Volts [28]. Fiala et al. studied the effect of adding carbon black to geopolymer,
66 at 2.25% by weight of slag, on the physical, mechanical, thermal, and electrical properties by
67 applying 40 and 100 DC volts; they obtained samples with compressive strength of 7.31 MPa,
68 electric conductivity of 1.3×10^{-1} S/m, and electrothermal performance of 44°C, 125°C at 40, 110
69 DC volts, respectively [19].

70 The mechanical strength of the pristine geopolymer utilized in some of these studies is already low,
71 as reported in [21,22] is due to the fact that the materials utilized are not really a geopolymer, based
72 on the precise definition of the geopolymer given by Joseph Davidovits [14], but they are alkali-

73 activated materials mistakenly called geopolymer, as many researchers use the two terms as
74 synonyms. Also, the electrothermal performance reported in these studies is noticeably weak as a
75 high voltage is required to produce low temperature, as reported in [19,28]. Moreover, the stability
76 of the electrothermal performance of the self-heating composites isn't reported in the literature.

77 It is well known that the geopolymer with a well-defined composition and structure has mechanical
78 strength higher than that of the alkali-activated materials [29]. Thus, if the geopolymer is prepared
79 with the right composition, it is expected that a suitable percent of carbon black can be incorporated
80 into it while maintaining acceptable mechanical strength for structural applications. Hence, a high
81 electrothermal performance can be achieved.

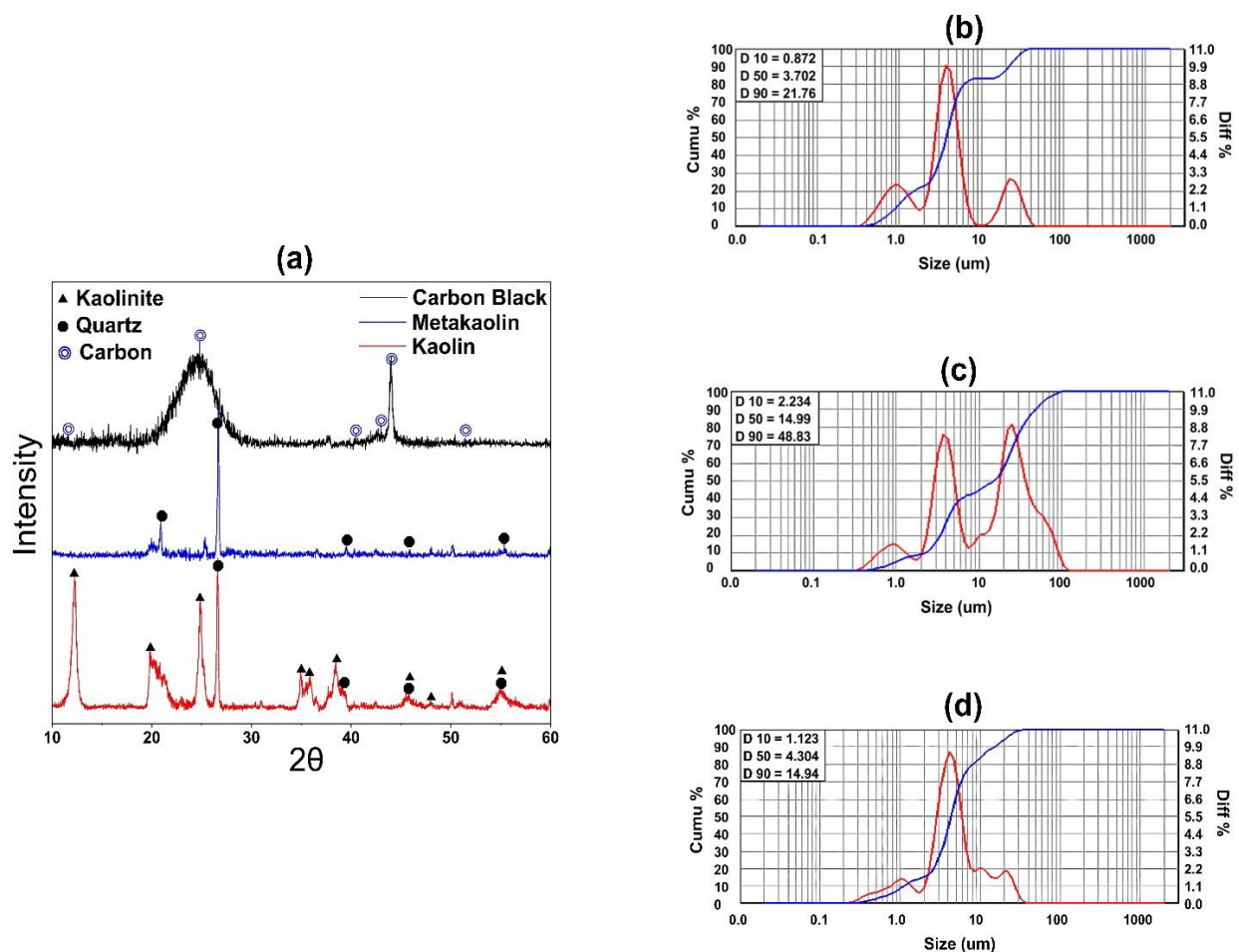
82 The current study investigates the effect of adding nano carbon black on the electrothermal
83 performance of metakaolin-based geopolymer as well as its mechanical, physical, and electrical
84 properties. Carbon black was added at a weight percent of 5%, 10%, 15%, and 20%, with respect
85 to the metakaolin content, and the compressive strength was measured at various ages of 7, 14, 28,
86 and 90 days. The electrothermal performance was tested using AC and DC voltages up to 12 V,
87 and the stability of this performance was also assessed.

88 **2. Materials and Methodology**

89 **2.1. Materials**

90 Metakaolin (SiO_2 w.t%= 54.46, Al_2O_3 w.t%= 33.68, Na_2O w.t%=0.22), nano carbon black powder
91 (N330, RPSG Group - India), industrial sodium hydroxide flakes (99% purity, from Al-Kout
92 Company - Kuwait), industrial sodium silicate solution (Na_2O w.t% = 13.1-13.7, SiO_2 w.t%= 32-
93 33, United Arab Emirates), copper tape with a width of 21 mm and a thickness of 0.1 mm used as
94 electrodes, and laboratory distilled water are the materials used for producing conductive
95 geopolymer samples. Metakaolin was produced from the calcination of kaolin (Supplied by Al-
96 Mishraq Company - Iraq) at a temperature of 800°C for three hours. **Figure 1(a)** shows the XRD

97 patterns of the kaolin, metakaolin, and carbon black; the diffraction data are in good agreement
 98 with the JCPDS cards (00-001-0527), (00-033-1161), and (01-074-2330) of the kaolinite, quartz,
 99 and carbon respectively. D_{50} for the kaolin, metakaolin, and carbon black is (3.702, 14.99, and
 100 4.304) μm , respectively, as can be seen in **Figure 1(b, c, d)**.



101
 102 **FIGURE 1** (a) XRD patterns of the kaolin, metakaolin, and carbon black; and the particle size
 103 distribution of the (b) kaolin, (c) metakaolin, and (d) carbon black

104
 105 **2.2. Methodology**

106 **2.2.1. Samples Preparation**

107 **Table 1** presents the weights of metakaolin (MK), carbon black-to-metakaolin ratio (CB/MK),
 108 sodium silicate-to-metakaolin ratio (SS/MK), sodium hydroxide-to-metakaolin ratio (SH/MK),
 109 and the water-to-metakaolin ratio (W/MK) used in the sample preparations for this study. For these

110 samples, the geopolymer has the formula $\text{Na}_2\text{O} \cdot \text{Al}_2\text{O}_3 \cdot 3.6\text{SiO}_2$, which was optimized in our
111 previous work to have a compressive strength of 117 MPa [30].

112 **TABLE 1** Samples ID and the composition of the samples

Sample ID	MK (g)	CB/MK	SS/MK	SH/MK	W/MK
GP-0	120.812	0	0.9755	0.0934	0.116
GP-1A	90.609	0.05	0.9755	0.0934	0.549
GP-1B	90.609	0.05	0.9755	0.0934	0.632
GP-1C	90.609	0.05	0.9755	0.0934	0.715
GP-2A	90.609	0.1	0.9755	0.0934	0.549
GP-2B	90.609	0.1	0.9755	0.0934	0.632
GP-2C	90.609	0.1	0.9755	0.0934	0.715
GP-3A	90.609	0.15	0.9755	0.0934	0.549
GP-3B	90.609	0.15	0.9755	0.0934	0.632
GP-3C	90.609	0.15	0.9755	0.0934	0.715
GP-4A	90.609	0.2	0.9755	0.0934	0.549
GP-4B	90.609	0.2	0.9755	0.0934	0.632
GP-4C	90.609	0.2	0.9755	0.0934	0.715

113
114 Sodium hydroxide (99% purity, Al-Kout Co. - Kuwait) solution was prepared by dissolving
115 sodium hydroxide flakes in 10 ml of laboratory distilled water, the desired amount of the sodium
116 silicate solution was added to the sodium hydroxide solution, and the solution was heated up to
117 $82 \pm 2^\circ\text{C}$ for 15 minutes, under stirring at a speed of 750 rpm, and it was left to cool before use.

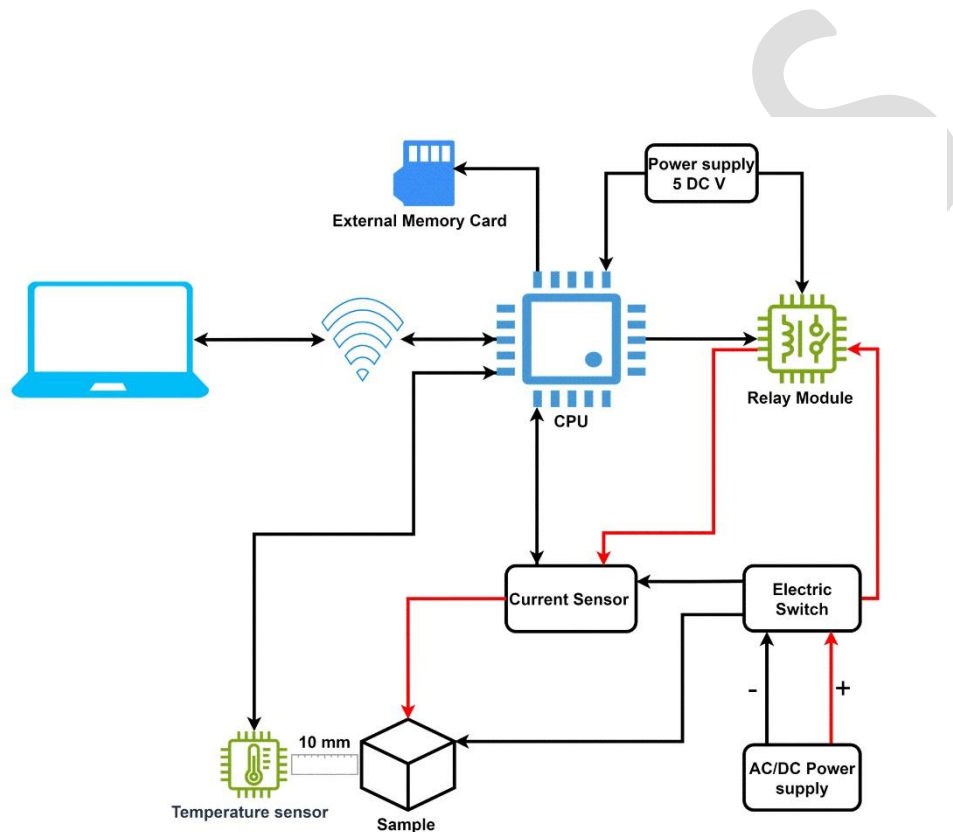
118 Carbon black (Industrial grade, N330, RPSG Group - India) powder was added to the solution
119 resulting from the previous step and mixed for 2 minutes at a speed of 700 rpm using an electronic
120 overhead stirrer (SL3000D - global lab. co). During mixing, water is added according to the
121 composition given in **Table 1**, excluding the 10 ml used to prepare the sodium hydroxide solution.
122 After that, the metakaolin powder was mixed with the mixture resulting from the previous step at

123 a speed of 3000 rpm for 5 minutes. The paste resulting from the previous step was poured into
124 molds made of silicone rubber, which are of three types: cylindrical molds with dimensions of
125 23x46 mm for testing compression strength, cubic molds with dimensions of 20x20x20 mm
126 containing two longitudinal slots on opposite sides, separated by 8 mm to fix copper electrodes,
127 used to investigating the electrical properties and electrothermal performance, and rectangular molds
128 with dimensions of 20x20x6 used for testing the physical properties and SEM examination. The
129 copper electrodes were installed after pouring the paste into the molds through the mold slots. The
130 samples were demolded after 72 hours and kept in the laboratory atmosphere at a temperature of
131 $18\pm 2^{\circ}\text{C}$ and relative humidity of 50% until the tests; all tests were conducted 28 days after
132 demolding the samples except the compression strength test, which is performed at different ages
133 of 7, 14, 28, and 90 days.

134 2.2.2. Characterization

135 The bulk density, true density, apparent porosity, and water absorption of the samples were tested
136 according to Archimedes' principle. An Impact-Automatic Console-2000 KN machine was used
137 to test the compressive strength of samples. SEM examination was used to investigate the
138 microstructural features of the samples using TESCAN- VEG 3 SBU nanospace machine. Hioki
139 IM 3536 device was used to measure impedance (Z), phase angle (θ), and electrical resistance
140 (R_{dc}). The EIS Spectrum Analysis software was also used to analyze the results and determine the
141 equivalent electrical circuit for the spectrum of the tested samples by using the NM Simp algorithm
142 and the Amplitude function. A direct and alternating voltage was applied to study the
143 electrothermal performance of the geopolymer/carbon black samples. A device consisting of a
144 processing unit board connected to a sensor for measuring current, a sensor for measuring the
145 surface temperature of the sample, and an AC/DC power supply, was used to detect the surface
146 temperature of the sample and the consumed current when a given voltage is applied. **Figure 2**

147 shows the test device schematic. The operation of the device is controlled via a computer, which
148 provides simultaneous measurement of current and temperature. The test voltage was selected
149 based on the electrical resistance of the samples. To avoid overheating, all samples were tested at
150 12 volts, with the exception of GP-4A, which was tested at 9 volts. A quick test with a single
151 heating cycle, 2 h of heating, and 0.5 an hour of cooling was conducted for all samples to determine
152 the electrothermal performance. Subsequently, selected samples were chosen and tested over three
153 cycles.



154
155 **FIGURE 2** A schematic of the test device

156 3. Results and Discussions

157 3.1. Physical Properties (Bulk and True density, apparent porosity, water absorption)

158 **Table 2** shows the values of the bulk density, true density, apparent porosity, and water absorption
159 of the samples; it can be noted that the geopolymer samples have higher density compared to the
160 composite samples that contain an additional percentage of carbon black. This is consistent with

161 studies showing that the incorporation of conductive filler can increase the porosity and reduce the
 162 bulk density of composite materials. While the relatively low density of carbon black may partially
 163 contribute to this effect, the increase in porosity is mainly attributed to its hydrophobic nature and
 164 the way it interacts with the binder matrix, and as the percentage of conductive filler increases, the
 165 pore size increases [31,32]. Also, it can be attributed to the low density of the carbon black as
 166 compared to the geopolymer, as well as the amount of water used to utilize the preparation of the
 167 composites seems to affect the density; part of this water is necessary to wet the carbon black and,
 168 hence, facilitate the preparation process while the residual amount of that water leads to the
 169 formation of more pores and, hence, lower bulk density. Also, this water works on impeding the
 170 polymerization process leading to lower true density for the geopolymer [33]. It can be noticed
 171 that the sample GP-3B has a lower porosity among the composites, indicating that it contains a
 172 lower amount of residual water. This is consistent with the study that shows that harmonizing the
 173 water / solid fraction leads to improving density [34].

174 **TABLE 2** The bulk density, true density, apparent porosity, and water absorption of the
 175 samples

Sample ID	Bulk density (g/cm ³)	True density (g/cm ³)	Apparent porosity (%)	Water absorption (%)
GP-0	1.5351	2.3495	34.6	22.5
GP-1A	1.2276	2.2208	44.7	36.4
GP-1B	1.1645	2.3177	49.7	42.7
GP-1C	1.1510	2.3347	50.6	44
GP-2A	1.2001	2.1531	44.2	36.8
GP-2B	1.1813	2.2250	46.9	39.7
GP-2C	1.1470	2.1855	47.5	41.4
GP-3A	1.1820	1.9343	38.8	32.9
GP-3B	1.1980	1.8673	35.8	29.9
GP-3C	1.1243	2.0628	45.4	40.4

GP-4A	1.1261	1.9316	41.6	37
GP-4B	1.1119	1.8754	40.7	36.6
GP-4C	1.1115	1.9835	43.9	39.5

176

177

178 3.2. Compressive Strength

179 **Figure 3** shows the compressive strength of geopolymer samples with different percent of carbon
 180 black. From **Figure 3(a)**, it is evident that the compressive strength of geopolymer samples is
 181 higher compared to those containing carbon black; this is because, in addition to the higher porosity
 182 of the composites, the carbon black is an inert phase within the geopolymer matrix that generates
 183 weak point via the aggregation [35], this can be clearly noticed in **Figure 3(b-e)** as the compressive
 184 strength at the age of 90 days of samples GP-1, GP-2, GP-3, and GP-4 are reduced due to the
 185 increase of the carbon black percent. Furthermore, there is a decrease in the compressive strength
 186 with increased water content for these samples due to the increase of the porosity. Notably, the
 187 samples GP-1 have the highest compressive strength among the composites due to their higher
 188 density.

189 Additionally, it has been observed that the increase in the compressive strength over time, which
 190 indicates the progress of the polymerization process, for GP-0 between 7 and 90 days is about
 191 26%. For the composites, this percent varies not only with the water content, which is known to
 192 impede the polymerization but also with the percent of the carbon black; this indicates that carbon
 193 black affects the polymerization process; however, investigating its role in this process requires
 194 further studies.

195 3.3. Scanning Electron Microscope Images

196 **Figure 4** shows the SEM images of the GP-0 sample. **Figure 4(a)** confirms the presence of a
197 continuous phase that is formed via the polymerization process; in this phase, different forms of
198 scraps are impeded, as appears more clearly in **Figures 4(b and c)**. This scrap can be assigned to
199 the inert phases that can't participate in the polymerization process. **Figure 4(d)** shows the un-
200 polished surface of the sample in which the pores and the drying microcracks are clearly appeared.
201 **Figures 5-7** show the microstructure of the composites. The aggregation of the carbon black is
202 observed in the composites; as the percent of the carbon black or the amount of water increases,
203 the size of the aggregates increases. Also, the images confirm the presence of microcracks that
204 pass through the geopolymer matrix, these cracks can be assigned to the drying of the surface of
205 the samples [36], and it can be noticed that the cracks pass through the carbon black aggregates,
206 **Figures 5a and 6a**, this indicates that the aggregates are weaker than the interface. Also, in the
207 case of high percent of carbon black, **Figures 6b, c and 7b, c**, a separation between the geopolymer
208 and the aggregates is noticed; this can be attributed to the hydrophobicity of the carbon black that
209 led to weak interaction with hydrophilic geopolymer matrix [37,38].

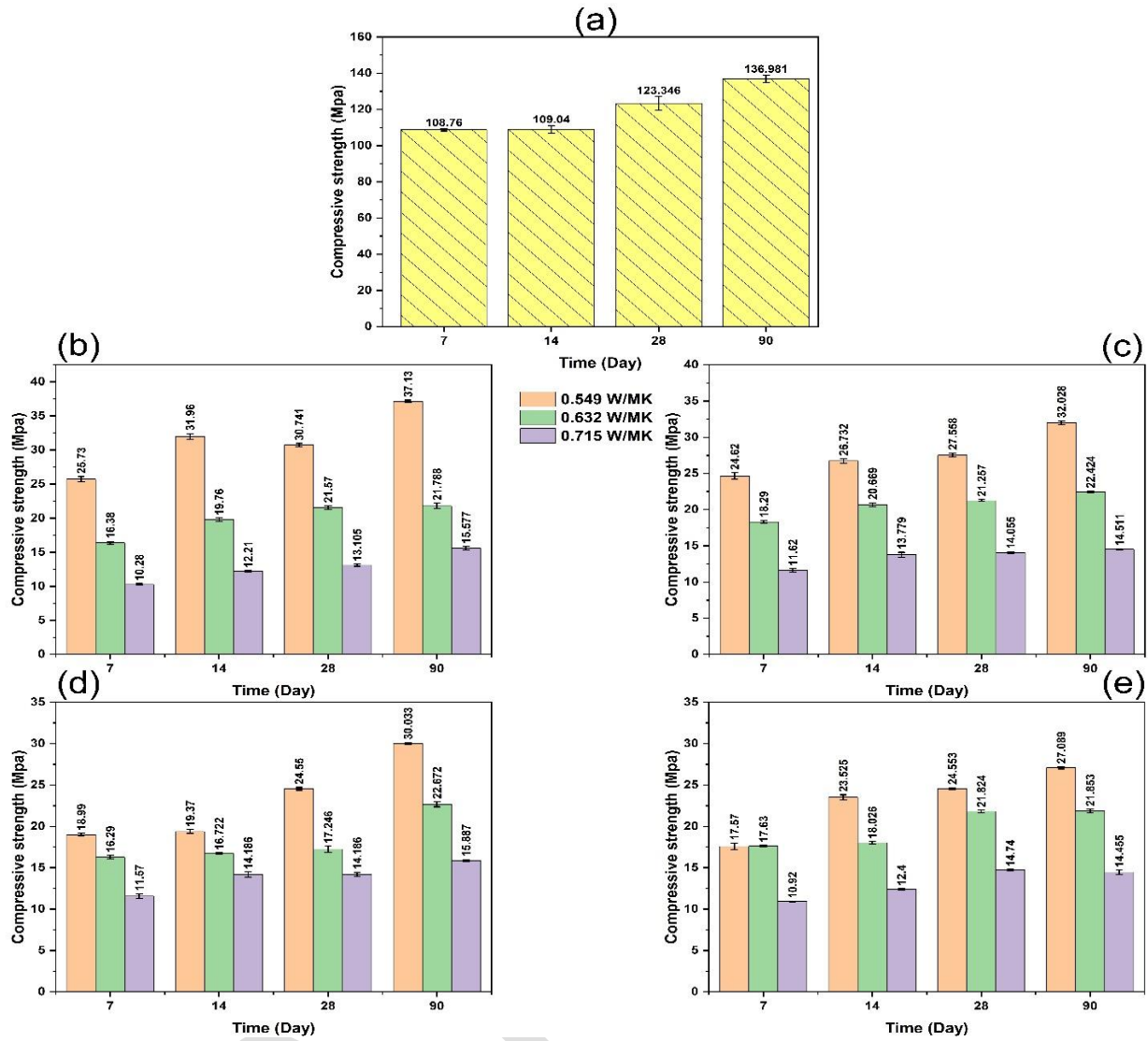


FIGURE 3 The compressive strength of geopolymer samples (a) GP-0, (b) GP-1, (c) GP-2, (d) GP-3, and (e) GP-4

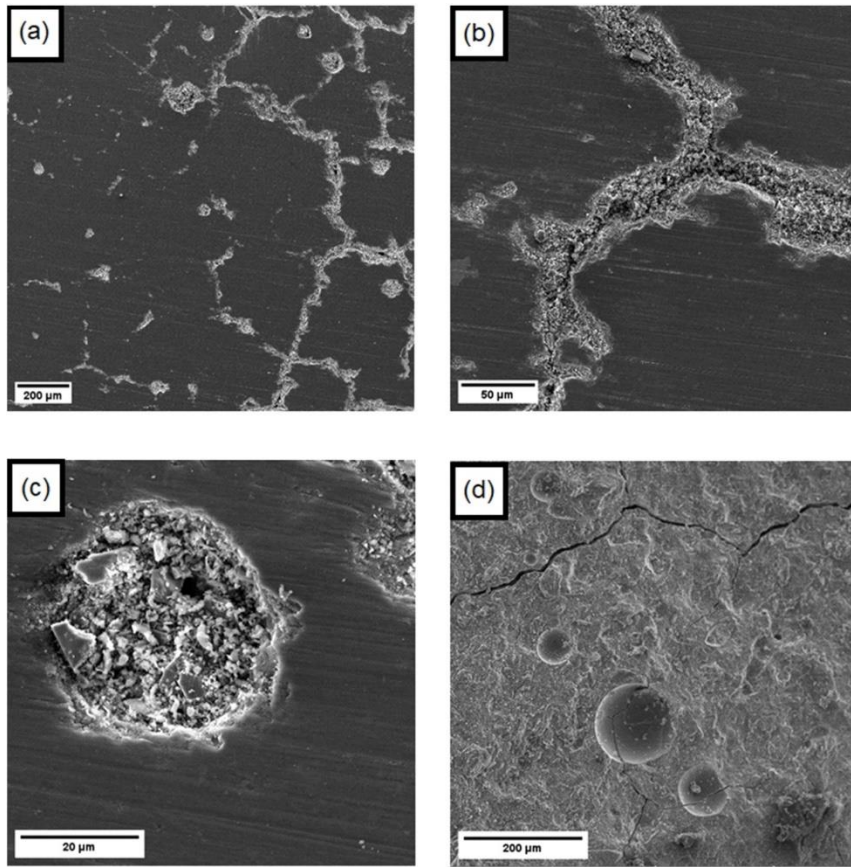
210

211

212

213

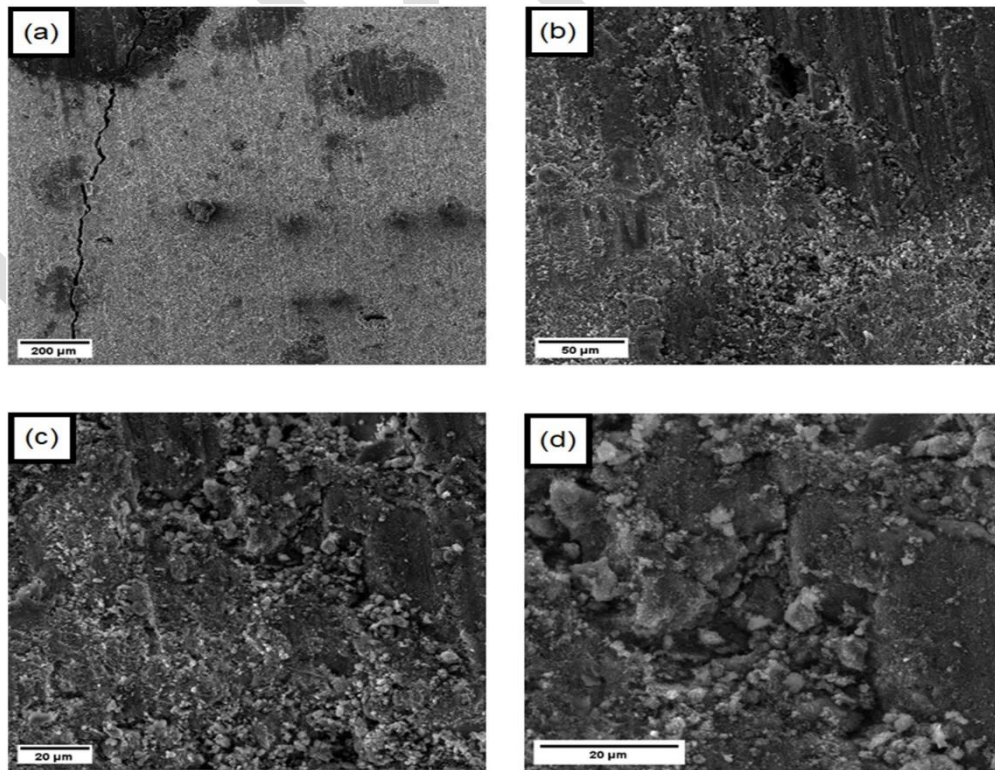
214



215

216

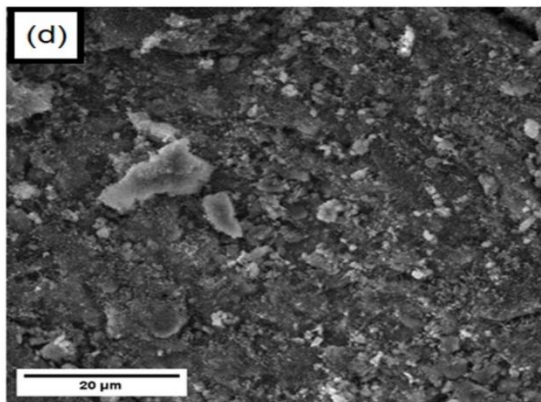
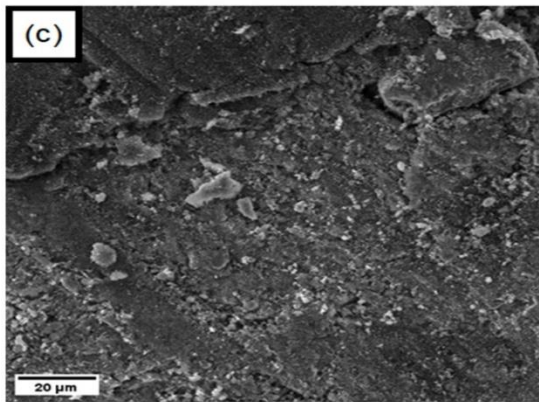
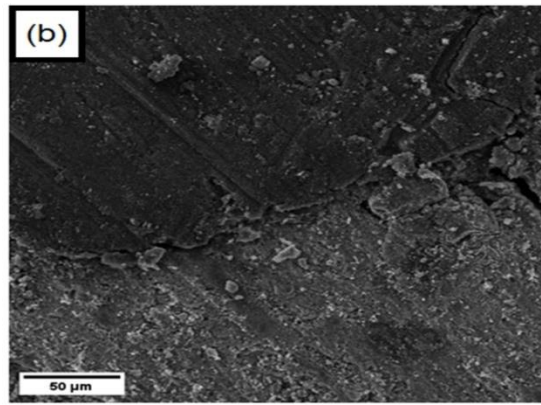
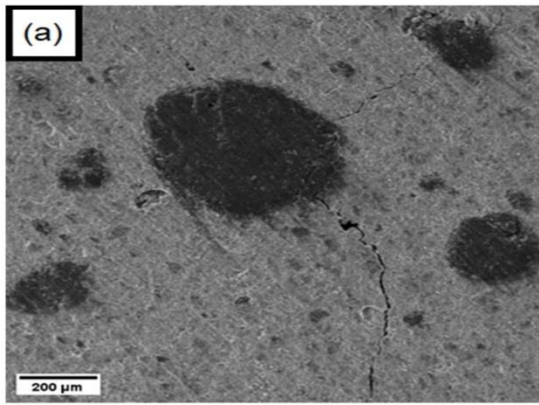
FIGURE 4 The SEM images of sample GP-0



217

218

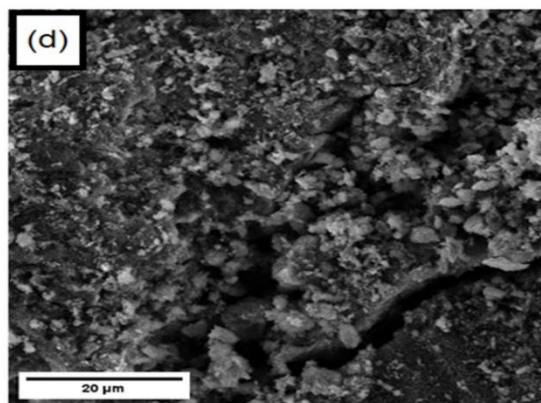
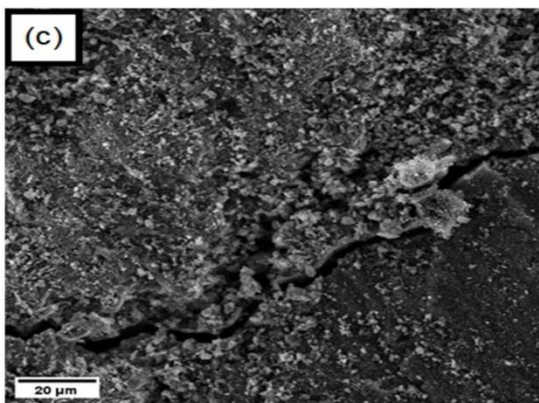
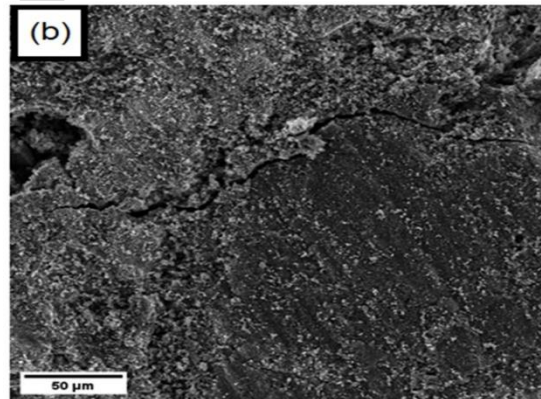
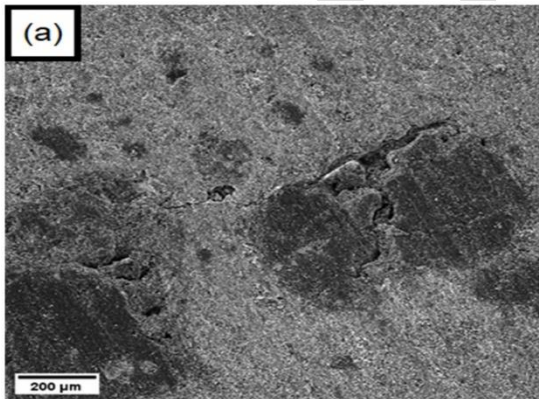
FIGURE 5 The SEM images of sample GP-2A



219

220

FIGURE 6 The SEM images of sample GP-2B



221

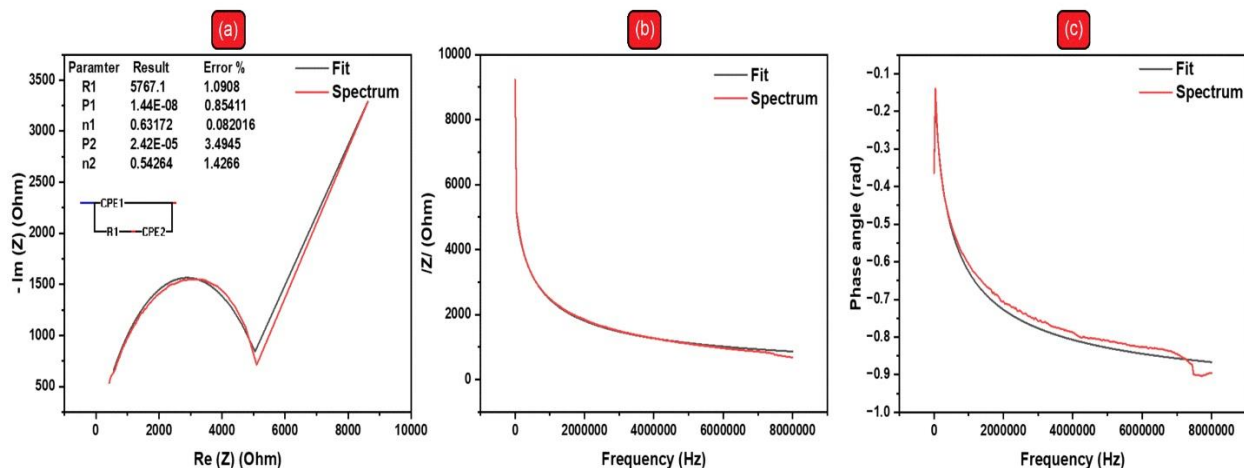
222

FIGURE 7 The SEM images of sample GP-4A

223

224 3.4. Electrochemical Impedance Spectroscopy

225 **Figure 8** shows the Nyquist plot, Bode plot, and the values of the phase angle for GP-0. It has
 226 been found, using the fitting and simulation of the Nyquist plot, that the equivalent electrical circuit
 227 that describes the geopolymer sample is $CPE_1 / (R_1 + CPE_2)$. This indicates that the material has a
 228 dielectric feature. As expected, the magnitude of impedance decreases with increasing frequency.
 229 Furthermore, the phase angle between voltage and current is negative, which is a characteristic of
 230 materials with capacitive behavior.



231

232 **FIGURE 8** Nyquist plot (a) and (b-c) Body plot from EIS of GP-0

233

234 **Figures 9** show the Nyquist plot, Bode plot, and the values of the phase angle for geopolymer
 235 composites with various carbon black percent. The equivalent electrical circuit that describes each
 236 composite is given below:

- 237 • GP-1A: $(CPE_1 / (R_1 + CPE_2 / R_2))$
- 238 • GP-1B: $CPE_1 / (R_1 / CPE_2)$
- 239 • GP-3C: $(R_1 / CPE_1 + (R_2 + CPE_2))$

240 • GP-4B: $(CPE_1/R_2) + (R_1/CPE_2)$

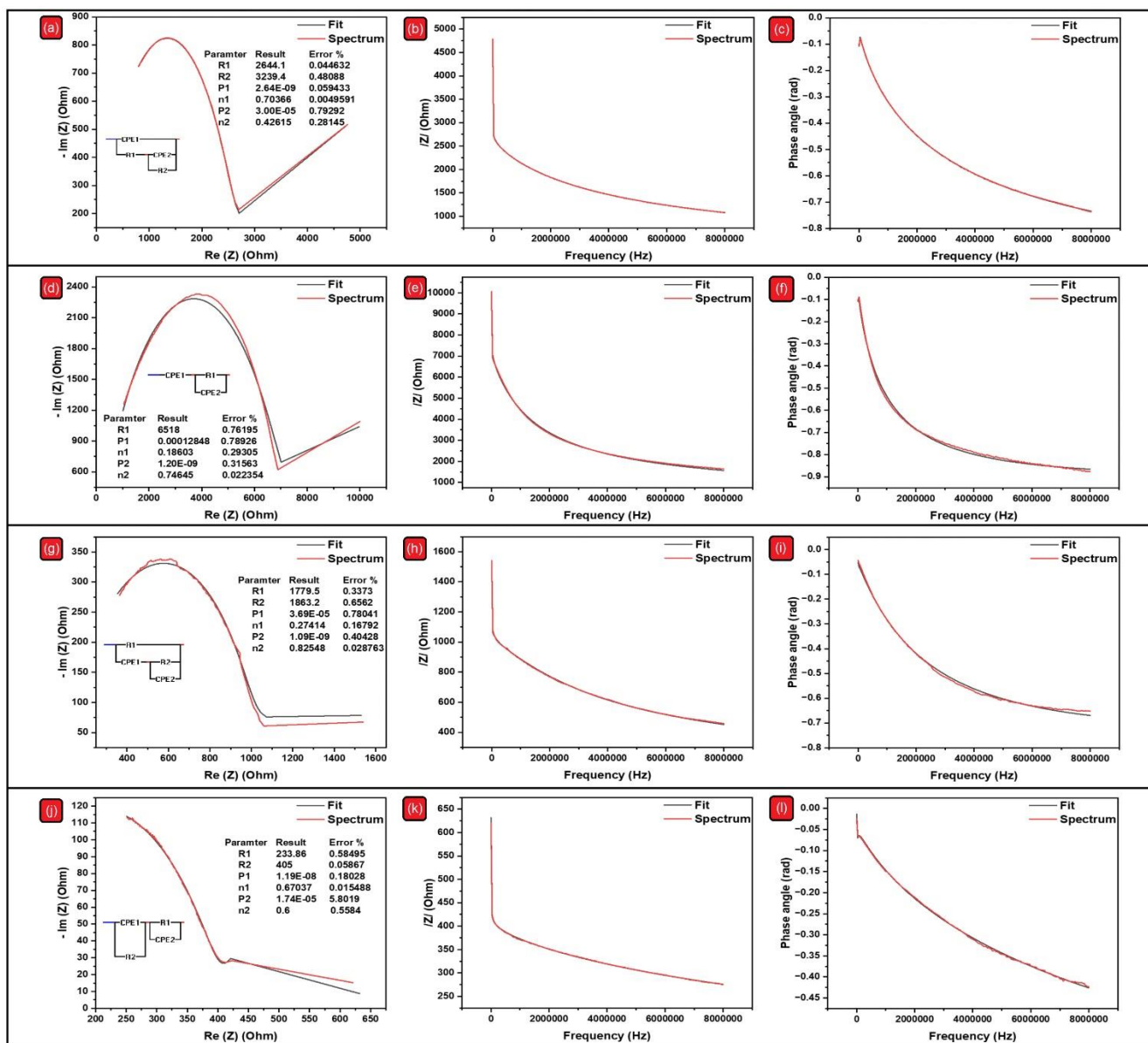
241 From the EIS results, the presence of more than one resistance in equivalent electrical circuits has
242 been noticed; this indicates the presence of more than one process area that affects the transfer of
243 charges. These resistances are the result of the simple ohmic resistance resulting from the flow of
244 current through the material, the resistance of the material, the resistance to the transfer of charge
245 from the electrode to the material, and the resistance to the diffusion of charges [39]. In addition,
246 the presence of more than one value for the constant phase element (CPE) was noticed; this
247 indicates the presence of electrical complexities within the material that affect the electrical
248 behavior; the causes of these complexities are electrochemical reactions on the surfaces of the
249 granules and the surfaces of the pores, corrosion reactions, and the presence of thin films [39].

250 It should be noted that the equivalent electrical circuit, which describes each of GP-1C, GP-2A,
251 GP-2B, and GP-2C, is the same equivalent electrical circuit that describes the sample GP-1B.
252 Similarly, the equivalent electrical circuit that describes each of GP-3A, GP-3B, and GP-4A is the
253 same equivalent electrical circuit that describes sample GP-3C. The GP-4C is described by the
254 same equivalent electrical circuit as the GP-4B. Also, it should be noted that only the values of the
255 elements forming the equivalent electrical circuit change with changes in the addition percent and
256 water content. This is due to the increased electrical complexities within the material resulting
257 from changes in density and porosity [39].

258 The Bode plots for GP-1, GP-2, GP-3, and GP-4 composites showed that the impedance decreases
259 with increasing frequency across all water content. As for the phase angle, it remains negative for
260 all samples at all frequencies; this behavior is due to the fact that the phase angle is negative,
261 meaning that the material has capacitive behavior.

262 3.5. Electric Resistance (R_{dc})

263 **Table 3** shows the electrical resistance values of geopolymer and geopolymer/carbon black
 264 composites. It is noted that the value of electrical resistance decreases with the increase in the
 265 percent of carbon black added; this is an expected result of the increase in conduction paths within
 266 the material.



267 **FIGURE 9** Nyquist plots (a, d, g, j) and (b-c; e-f; h-i; k-l) Bode plots from EIS of GP-1A,
 268 GP-1B, GP-3C, GP-4B, respectively.
 269

270
 271 It is also noted that the value of electrical resistance increases with increasing water content, and
 272 this behavior is due to the increase in porosity, which is observed in all samples except for (GP-

273 2B, GP-3B, GP-4B), where there is a heterogenous distribution of additive within the samples, as
 274 appear more clearly in **Figures 10**. The electrical resistance of the composites is the result of the
 275 (i) formation of the conductive paths that reduce the electrical resistance, (ii) the presence of the
 276 pores filled with carbon black, which behave as a junction that facilitates the connection between
 277 the conductive paths, and (iii) the presence of empty pores which cut the conductive paths. The
 278 time factor must be taken into consideration when examining electrical resistance, as its value
 279 increases with time as a result of the loss of water that participates in the electrical conduction
 280 process as the polymerization process continues [40], or its value decreases with the loss of water
 281 present in the pores, and thus the conductive filler agglomerates and forms additional paths [41].

282 **TABLE 3** The values of the electrical resistance of the samples

Sample ID	Rdc (Ω)	Sample ID	Rdc (Ω)
GP-0	8638	GP-3A	497.655
GP-1A	4307.18	GP-3B	919.06
GP-1B	8995.58	GP-3C	1413.838
GP-1C	12508.2	GP-4A	142.009
GP-2A	2549.53	GP-4B	535.039
GP-2B	8657.59	GP-4C	675.497
GP-2C	4060.5		

283

284

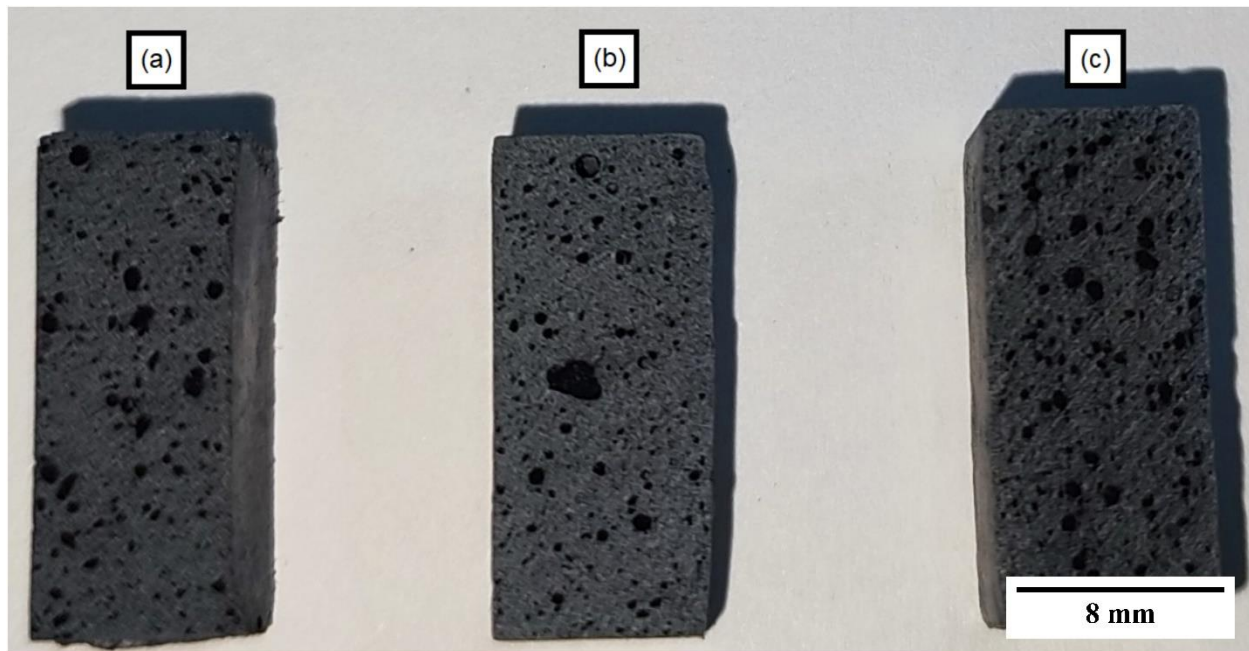


FIGURE 10 Distribution of carbon black (a) GP-2A, (b) GP-2B, (c) GP-2C

3.6. Electrothermal Performance

Due to the high electrical resistance of the GP-0, its electrothermal effect hasn't a practical value.

Figure 11 shows the electrothermal effect of the geopolymer composites tested over a single heating cycle of two hours and a cooling period of half an hour, with both AC and DC voltages. It

has been found that GP-1 samples can reach a temperature of around 32.75°C, GP-2 samples achieve a temperature of 32-34°C, GP-3 samples reach a temperature of 34-44°C, and GP-4

samples achieve a temperature of 37-50°C by an applied voltage of 12 volts, with the exception of GP-4A sample that reaches to a temperature of 62°C by an applied voltage of 9 volts. It has been

observed that the electrothermal effect with AC voltage is better when compared to DC voltage.

Also, the consumed energy in the case of DC voltage is found to be higher than that consumed when AC voltage is applied, and this is because of the Joule effect. Also, it has been observed that

the higher the amount of water used in the preparation of the sample, the lower the electrothermal

effect obtained; this is related to the higher porosity obtained and, hence, the higher electrical

resistance achieved.

285

286

287

288

289

290

291

292

293

294

295

296

297

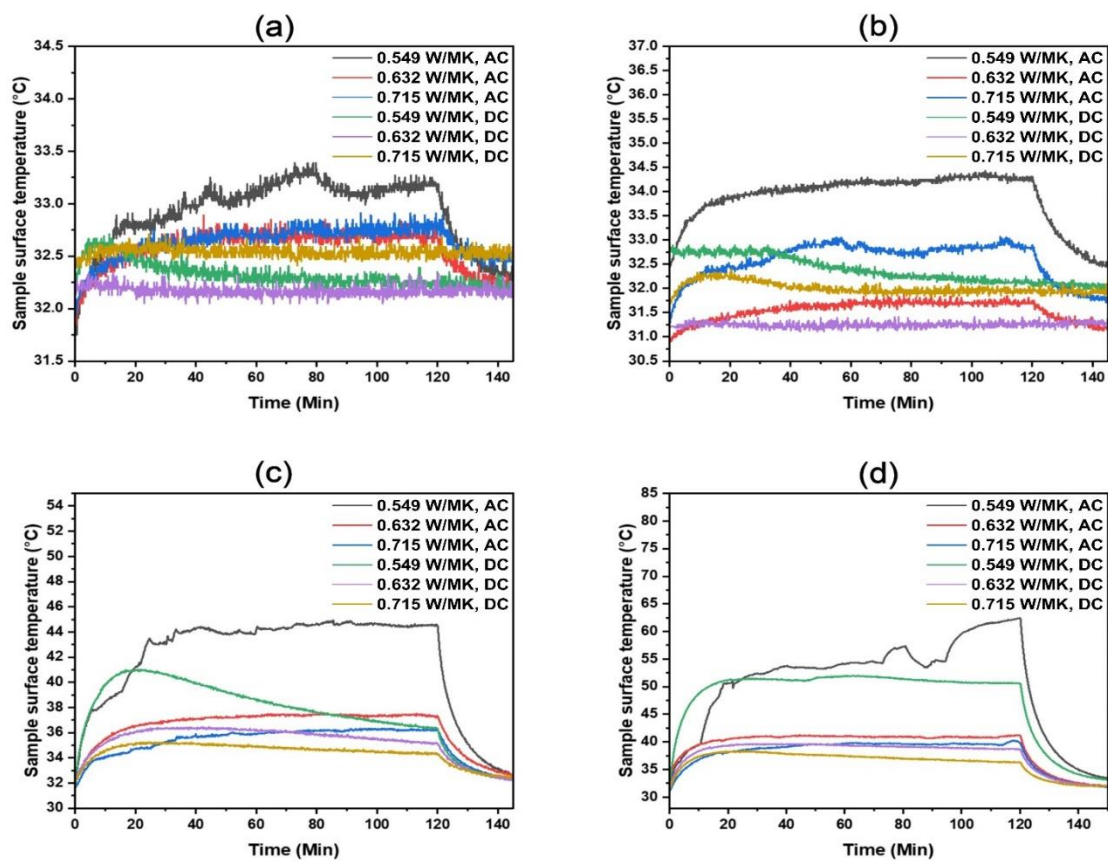
298

299

300

301 An important issue was noticed regarding the stability of the electrothermal performance of the
302 samples. It has been observed that the samples gradually lose their ability to convert the electrical
303 field into heat. The rate at which this happens depends on the type of the applied voltage; the AC
304 voltage reduces that rate lower than the DC voltage. This indicates that something is changed in
305 the electric circuit when the electric field is applied. Keep in mind that the mechanisms of electrical
306 conduction in geopolymer depend either on the movement of sodium or potassium ions, the
307 movement of free electrons, or the movement of hydroxide ions resulting from the water content
308 when an electric field is applied [42–44]. Two possible reasons can explain this: the first is the
309 increase of the electrical resistance due to the destruction of the conductive paths, and the second
310 is the generation of a barrier between the sample and the electrode. Zhang et al. claimed that the
311 decrease in the electrothermal effect of a sample containing 100 w.t% graphite, whose
312 electrothermal performance was tested at 7 days, is due to the first reason: they suggested that the
313 evaporation of water during the heating cycle leads to a shrinkage of the gel in the geopolymer
314 and, consequently, to a destruction of the conduction network [45]. However, such a scenario may
315 be accepted for the samples at an early age, when the polymerization process is going on and its
316 byproduct, water, is formed. Nevertheless, that scenario is less probable when the sample is tested
317 after the age of 28 days.

318 In the current study, it has been found that a barrier layer is formed between the copper electrode
319 and the sample surface, as shown in Figure 12; after removing this layer via polishing, the circuit
320 restored its electrothermal performance. The presence of this layer suggests that there are mobile
321 ions in the sample that can be drifted via the electric field and react with the copper electrode to
322 form that layer. The presence of such ions in the geopolymer was proved by Cui et al. [46].



323
 324 **FIGURE 11** The electrothermal effect of geopolymer samples (a) GP-1; (b) GP-2; (c) GP-3;
 325 (d) GP-4



326
 327 **FIGURE 12** The barrier layer formed between the electrode and the sample

328
 329 In order to support this scenario, the electrothermal behavior was evaluated after immersing the
 330 samples in deionized water for 24 hours to remove the free ions and drying them at 100°C for 3
 331 hours. **Figure 13** illustrates the electrothermal behavior of the chosen samples over three cycles;

332 it can be seen that the electrothermal behavior of the sample is noticeably stable over the three
333 cycles; this confirms that the formation of the barrier layer is the reason behind the loss of the
334 electrothermal behavior of the samples. It should be noted that the electrical resistance of samples
335 GP3-A and GP-4A decreased after removing the free ions to become 141.5 and 23.4 ohms,
336 respectively, and a temperature of 58 and 142°C could be achieved using 12 and 9V DC. This
337 electrothermal performance is superior as compared to that reported in the literature [19,28,45].

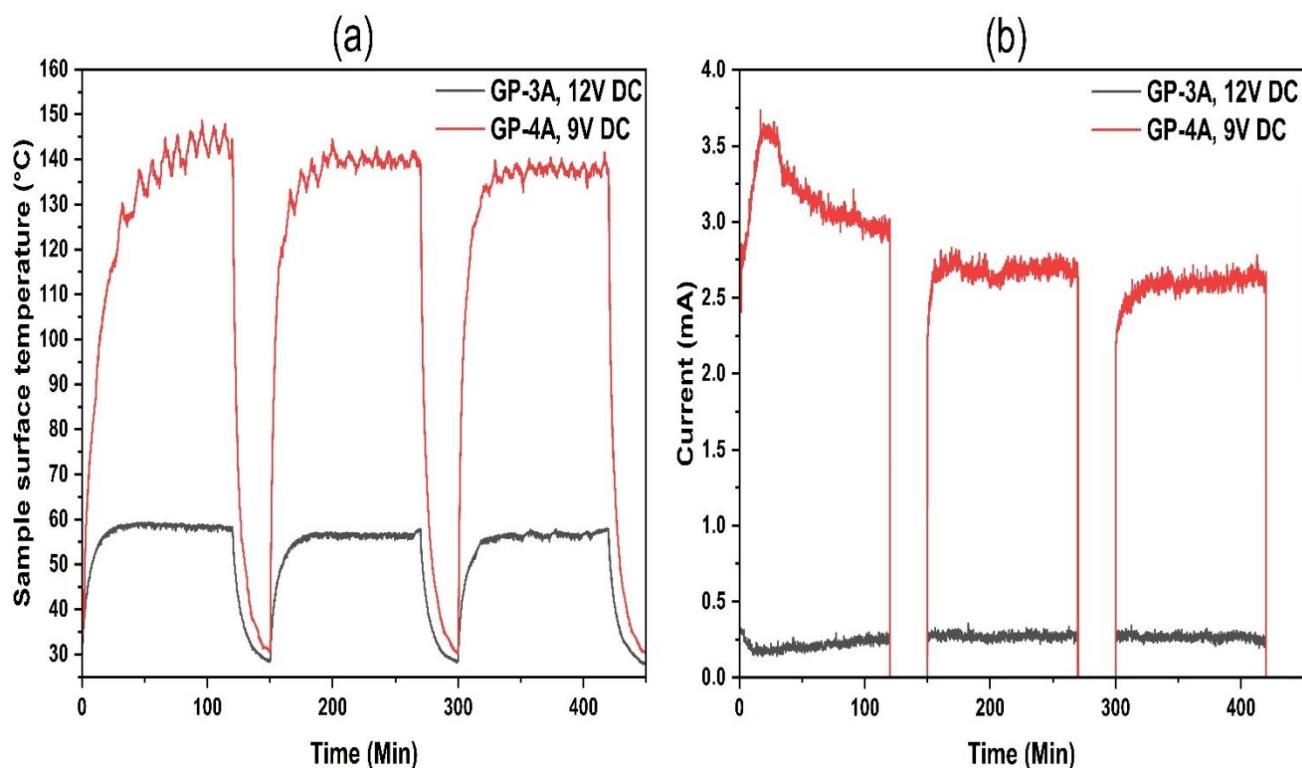
338

339 **4. Conclusion**

340 The current study aimed to study the effect of adding carbon black to the metakaolin-based
341 geopolymer. The following conclusions can be driven:

- 342 1- With the increase in the addition of carbon black, the compressive strength decreases and
343 the electrical conductivity increases. However, using the right formula of the geopolymer
344 along with the balance between the carbon black percent and the lowest water content
345 possible, a conductive geopolymer with high compressive strength can be obtained.
- 346 2- The electrothermal performance of conductive geopolymer samples can be improved by
347 increasing the percent of the carbon black and lowering the water content. However,
348 increasing the addition percent increases energy consumption; thus, a compromise is
349 needed between the desired temperature and the energy consumption. Additionally, the
350 electrothermal performance is better with AC voltage compared to DC voltage applied.

351 The reason for the deterioration of the electrothermal performance is the formation of a barrier
352 layer between the electrode and the sample surface. This can be avoided by removing the free ions
353 from the sample via washing.



35.
 355 **FIGURE 13** (a) electrothermal behavior and (b) energy consumption of GP-3A, GP-4A after
 356 removing the free ions

357 5. Recommendation

359 It is recommended to carefully evaluate the homogeneity of the composite geopolymer and
 360 to perform measurements of the compressive strength, electrical performance and
 361 electrothermal performance of the homogeneous geopolymer well to ensure the reliability
 362 of performance assessment.

363 6. Reference

- 364 [1] Jwaida Z, Dulaimi A, Mashaan N, Othuman Mydin MA. "Geopolymers: The green
 365 alternative to traditional materials for engineering applications". Infrastructures (Basel).
 366 2023, 8–98.
 367 [2] Bai C, Colombo P. "Processing, properties and applications of highly porous geopolymers: A
 368 review". Ceram Int. 2018, 44, 16103–18.
 369

- 370 [3] Duan P, Yan C, Zhou W, Luo W, Shen C. "An investigation of the microstructure and
371 durability of a fluidized bed fly ash–metakaolin geopolymer after heat and acid exposure".
372 Mater Des. 2015, 74, 125–37.
- 373 [4] Hassan A, Arif M, Shariq M. "A review of properties and behaviour of reinforced
374 geopolymer concrete structural elements-A clean technology option for sustainable
375 development". J Clean Prod. 2020, 245–118762.
- 376 [5] de Toledo Pereira DS, da Silva FJ, Porto ABR, Candido VS, da Silva ACR, Garcia Filho
377 FDC, Monteiro SN. "Comparative analysis between properties and microstructures of
378 geopolymeric concrete and portland concrete". Journal of Materials Research and
379 Technology. 2018, 7, 606–11.
- 380 [6] Karthik A, Sudalaimani K, Vijayakumar CT. "Durability study on coal fly ash-blast furnace
381 slag geopolymer concretes with bio-additives". Ceram Int. 2017, 43, 11935–43.
- 382 [7] Turner LK, Collins FG. "Carbon dioxide equivalent (CO₂-e) emissions: A comparison
383 between geopolymer and OPC cement concrete". Constr Build Mater. 2013, 43, 125–30.
- 384 [8] Paruthi S, Husain A, Alam P, Khan AH, Hasan MA, Magbool HM. "A review on material mix
385 proportion and strength influence parameters of geopolymer concrete: Application of ANN
386 model for GPC strength prediction". Constr Build Mater. 2022, 356–129253.
- 387 [9] Taki K, Mukherjee S, Patel AK, Kumar M. "Reappraisal review on geopolymer: A new era
388 of aluminosilicate binder for metal immobilization". Environ Nanotechnol Monit Manag.
389 2020, 14–100345.
- 390 [10] Tan TH, Mo KH, Ling T-C, Lai SH. "Current development of geopolymer as alternative
391 adsorbent for heavy metal removal". Environ Technol Innov. 2020, 18–100684.
- 392 [11] He P, Cui J, Wang M, Fu S, Yang H, Sun C, Duan X, Yang Z, Jia D, Zhou Y. "Interplay
393 between storage temperature, medium and leaching kinetics of hazardous wastes in
394 Metakaolin-based geopolymer". J Hazard Mater. 2020, 384–121377.
- 395 [12] Jiang C, Wang A, Bao X, Ni T, Ling J. "A review on geopolymer in potential coating
396 application: Materials, preparation and basic properties". Journal of Building Engineering.
397 2020, 32–101734.
- 398 [13] Lahoti M, Tan KH, Yang E-H. "A critical review of geopolymer properties for structural
399 fire-resistance applications". Constr Build Mater. 2019, 221, 514–26.

- 400 [14] Davidovits J. "Geopolymers: Ceramic-like inorganic polymers". *J Ceram Sci Technol*.
401 2017, 8, 335–50.
- 402 [15] Dai S, Wang H, An S, Yuan L. "Mechanical properties and microstructural characterization of
403 metakaolin geopolymers based on orthogonal tests". *Materials*. 2022, 15–2957.
- 404 [16] Rashad AM. "A comprehensive overview about the influence of different additives on the
405 properties of alkali-activated slag—A guide for Civil Engineer". *Constr Build Mater*. 2013,
406 47, 29–55.
- 407 [17] Rashad AM. "Alkali-activated metakaolin: A short guide for civil Engineer—An overview".
408 *Constr Build Mater*. 2013, 41, 751–65.
- 409 [18] Irshidat MR, Al-Nuaimi N, Rabie M. "Sustainable utilization of waste carbon black in
410 alkali-activated mortar production". *Case Studies in Construction Materials*. 2021, 15–
411 e00743.
- 412 [19] Fiala L, Petříková M, Lin W-T, Podolka L, Černý R. "Self-heating ability of geopolymers
413 enhanced by carbon black admixtures at different voltage loads". *Energies (Basel)*. 2019, 12–
414 4121.
- 415 [20] Vlachakis C, Wang X, Al-Tabbaa A. "Investigation of the compressive self-sensing
416 response of filler-free metakaolin geopolymer binders and coatings". *Constr Build Mater*.
417 2023, 392–131682.
- 418 [21] Mizerová C, Kusák I, Rovnaník P, Bayer P. "Metakaolin/carbon black geopolymer with
419 enhanced electrical properties". *IOP Conf Ser Mater Sci Eng*. vol. 549, IOP Publishing,
420 2019, p. 012033.
- 421 [22] Mizerová C, Kusák I, Rovnaník P. "Application of carbon black in conductive fly ash
422 geopolymer mortars". *IOP Conf Ser Mater Sci Eng*. vol. 583, IOP Publishing, 2019, p.
423 012014.
- 424 [23] Arif FT, Heryanto H, Sulieman A, Bradley DA, Tahir D. "Geopolymer cellulose-based
425 composite Black Carbon (BC)/Fe/Cu/polyvinyl alcohol for eco-friendly apron X-ray".
426 *Radiation Physics and Chemistry*. 2023, 207–110843.
- 427 [24] Rauf N, Darmawan ZT, Ilyas S, Heryanto H, Fahri AN, Rahmat R, Abdullah B, Tahir D. "Effect
428 of Fe₃O₄ in enhancement optical and gamma ray absorption properties of geopolymer apron
429 cassava starch/black carbon/glycerin". *Opt Mater (Amst)*. 2021, 113–110887.
- 430 [25] Gu G, Ma T, Chen F, Han C, Li H, Xu F. "Co-modifying geopolymer composite by nano
431 carbon black and carbon fibers to reduce CO₂ emissions in airport pavement induction
432 heating". *Compos Part A Appl Sci Manuf*. 2024, 177–107951.

- 433 [26] Han J, Pan J, Wang X, Cai J, Gu L, Yang J. "Conductive behavior of engineered geopolymer
434 composite with addition of carbon fiber and nano-carbon black". *Ceram Int.* 2023, 49, 32035–
435 48.
- 436 [27] Mizerová C, Kusák I, Topolář L, Schmid P, Rovnaník P. "Self-sensing properties of fly ash
437 geopolymer doped with carbon black under compression". *Materials.* 2021, 14–4350.
- 438 [28] Cai J, Li X, Tan J, Vandevyvere B. "Fly ash-based geopolymer with self-heating capacity
439 for accelerated curing". *J Clean Prod.* 2020, 261–121119.
- 440 [29] Wardhono A, Law DW, Molyneaux TCK. "Strength of alkali activated slag and fly ash-
441 based geopolymer mortar". *Proceedings of Microstructural-Related Durability of*
442 *Cementitious Composites, Microdurability.* 2012.
- 443 [30] Alnasur MSH, Al-hydary IAD. "Development of Lightweight Geopolymer Concrete:
444 Strength and Density Studied". *Journal of University of Babylon for Engineering Sciences.*
445 2023, 31, 15–25.
- 446 [31] Mizerová C, Kusák I, Rovnaník P. "Electrical properties of fly ash geopolymer composites
447 with graphite conductive admixtures". *Acta Polytech CTU Proc.* 2019, 22, 72–6.
- 448 [32] Hotěk P, Fiala L, Černý R. "Thermoelectric properties of metashale geopolymer mortar
449 doped with graphite powder". *J Phys Conf Ser.* vol. 2628, IOP Publishing. 2023, p. 012006.
- 450 [33] Dubyey L, Ukrainczyk N, Yadav S, Izadifar M, Schneider JJ, Koenders E. "Carbon
451 nanotubes and nanohorns in geopolymers: A study on chemical, physical and mechanical
452 properties". *Mater Des.* 2024, 240–112851.
- 453 [34] Agustini NKA, Triwiyono A, Sulisty D. "Effects of water to solid ratio on thermal
454 conductivity of fly ash-based geopolymer paste". *IOP Conf Ser Earth Environ Sci.* vol. 426,
455 IOP Publishing. 2020, p. 012010.
- 456 [35] Zhang Y, He P, Yuan J, Yang C, Jia D, Zhou Y. "Effects of graphite on the mechanical and
457 microwave absorption properties of geopolymer based composites". *Ceram Int.* 2017, 43,
458 2325–32.
- 459 [36] Kuenzel C, Vandeperre LJ, Donatello S, Boccaccini AR, Cheeseman C. "Ambient
460 temperature drying shrinkage and cracking in metakaolin-based geopolymers". *Journal of*
461 *the American Ceramic Society.* 2012, 95, 3270–7.

- 462 [37] Li Y, Zhang W, Zhao J, Li W, Wang B, Yang Y, Sun J, Fang X, Xia R, Liu Y. "A route of
463 alkylated carbon black with hydrophobicity, high dispersibility and efficient thermal
464 conductivity". *Appl Surf Sci.* 2021, 538–147858.
- 465 [38] Zhang D, Zhu H, Wu Q, Yang T, Yin Z, Tian L. "Investigation of the hydrophobicity and
466 microstructure of fly ash-slag geopolymer modified by polydimethylsiloxane". *Constr
467 Build Mater.* 2023, 369–130540.
- 468 [39] Lasia A. *Electrochemical Impedance Spectroscopy and its Applications.* Springer. New
469 York, 2014.
- 470 [40] Payakaniti P, Pinitsoontorn S, Thongbai P, Amornkitbamrung V, Chindaprasirt P.
471 "Electrical conductivity and compressive strength of carbon fiber reinforced fly ash
472 geopolymeric composites". *Constr Build Mater.* 2017, 135, 164–76.
- 473 [41] Zhang S, Ukrainczyk N, Zaoui A, Koenders E. "Electrical conductivity of geopolymer-
474 graphite composites: Percolation, mesostructure and analytical modeling". *Constr Build
475 Mater.* 2024, 411–134536.
- 476 [42] Cai J, Pan J, Li X, Tan J, Li J. "Electrical resistivity of fly ash and metakaolin based
477 geopolymers". *Constr Build Mater.* 2020, 234–117868.
- 478 [43] Zhang Y, Chen S, Liang T, Ruan S, Wang W, Lin J, Liu Y, Yan D. "EIS investigation on
479 electrical properties of metakaolin-based geopolymer". *Constr Build Mater.* 2024, 437–
480 136851.
- 481 [44] Sellami M, Barre M, Toumi M. "Synthesis, thermal properties and electrical conductivity
482 of phosphoric acid-based geopolymer with metakaolin". *Appl Clay Sci.* 2019, 180–105192.
- 483 [45] Zhang Y, Lin J, Chen S, Ruan S, Wang W, Liu Y, Yan D. "Electrothermal effect of carbon
484 fiber and graphite reinforced metakaolin-based geopolymer". *Int J Appl Ceram Technol.*
485 2024.
- 486 [46] Cui X-M, Zheng G-J, Han Y-C, Su F, Zhou J. "A study on electrical conductivity of
487 chemosynthetic $Al_2O_3-2SiO_2$ geopolymer materials". *J Power Sources.* 2008, 184, 652–6.
488